The current issue and full text archive of this journal is available at
www.emeraldinsight.com/0961-5539.htm

Received 29 September 2007
Revised 19 December 2007
Accepted 19 December 2007

Jet impingement onto a cylindrical cavity

Effect of jet velocity on heat transfer and skin friction

B.S. Yilbas and S.Z. Shuja
ME Department, KFUPM, Dhahran, Saudi Arabia

Abstract

Purpose – The paper's aim is to provide information on heat transfer and flow characteristics for a jet emerging from a conical nozzle and impinging onto the cylindrical, which resembles the laser heating process, for researchers and graduate students working in the laser processing area, which can help them to improve the understanding of the laser machining process.

Design/methodology/approach – A numerical scheme employing the control volume approach is introduced to model the flow and heating situations. The effect of jet velocity on the heat transfer rates and skin friction around the cylindrical cavity subjected to the jet impingement was investigated.

Findings – Increasing jet velocity at nozzle exit enhances the heat transfer rates from the cavity wall and modifies the skin friction at cavity wall, which is more pronounced as the cavity depth increases to 1 mm.

Research limitations/implications – The effects of nozzle cone angle on the flow structure and heat transfer characteristics were not examined, which perhaps limits the general usefulness of the findings.

Practical implications – Very useful information are provided for the laser gas assisted processing, which has a practical importance in machining industry.

Originality/value – This paper provides original information for the effects of the gas jet velocity on the cooling rates of the laser produced cavity.

Keywords Heat transfer, Friction, Jets, Fluid power cylinders, Flow

Paper type Research paper

Nomenclature

H	enthalpy	t	time
K	thermal conductivity	T	temperature
k	turbulent kinetic energy	u*	friction velocity
p	pressure	U	arbitrary velocity
P	rate of production	$\forall$	volume
R_{ij}	Reynolds stress	x	distance in the axial direction
Re	Reynolds number	x_n	distance to the nearest wall
r	distance in the radial direction	x_{max}	distance to the solid rear surface

International Journal of Numerical Methods for Heat & Fluid Flow
Vol. 19 No. 2, 2009
pp. 182-200

0961-5539
DOI 10.1108/09615530910930964

The authors acknowledge the support of King Fahd University of Petroleum and Minerals, Dhahran, Saudi Arabia.

Greek

α	thermal diffusivity
Γ	arbitrary diffusion coefficient
ϵ	energy dissipation
λ	turbulence intensity
μ	dynamic viscosity
ν	kinematic viscosity
ρ	density (function of temperature and pressure for gas)
σ	variable Prandtl number
Φ	viscous dissipation
ϕ	arbitrary variable
Π	energy transport due to pressure excluding strain interactions
Π^w	energy transport due to wall reflection
Λ	energy transport by diffusion

subscript

amb	ambient
i, j	arbitrary direction
jet	gas jet at inlet
l	laminar
p	a typical node in the computational grid
t	turbulent
n, s, e, w, l, h	north, south, east, west, low or high node
w	wall

1. Introduction

Conical nozzles are used in laser machining applications; in which case, the assisting gas emerges from a nozzle and impinges onto the workpiece surface. Depending on the nozzle geometry and the flow conditions at the nozzle exit, the flow structure developed between the nozzle and the workpiece changes. This, in turn, alters the assisting gas effect on the laser machining process through modifying the heat transfer rates from the laser machined section. However, experimentation of such flow situation is expensive and involves with high-temperature phenomena, which may not be captured with required accuracy. However, a model study of such situation provides insight into the physical processes taking place during the gas impingement onto the substrate surfaces. Moreover, the flow field is turbulent because of the high jet Reynolds number; therefore, the turbulence model should be accommodated in the study. Consequently, investigation into the jet impingement onto the surface and effects of geometric configurations of nozzle and nozzle exit velocity on heat transfer rates as well as skin friction becomes necessary.

Considerable research studies were carried out to examine laser gas assisting processes using the nozzles. The dynamic characteristics of gas flow inside a laser cut kerf under high assisting gas pressure were studied by Man *et al.* (1997). They indicated that the sensitivity to the stand-off distance and the workpiece thickness of supersonic nozzle were much less as compared with the conical nozzle subsonic nozzle. The effects of high-pressure assisting gas on the laser cutting process were examined by Chen (1998). He showed that the high-quality cutting was not possible for the use of pure oxygen assisting gas and the nozzle stand-off spacing had significant effect on the cutting quality. Yilbas *et al.* (2002) investigated laser gas assisted processing in relation to machining. They showed that assisting gas pressure had significant effect on the end product quality. Yilbas and Aleem (2006) formulated the effect of assisting gas on the liquid layer thickness and correlated the liquid layer thickness with the dross size, which was ejected from the kerf side.

Considerable research studies were carried out to examine heat transfer rates from the surfaces due to jet impingement. Ashforth-Frost and Jambunathan (1996) studied semi-confined jet impingement onto the surfaces. They indicated that the model employed to account for the turbulence had significant effect on the heat transfer rates from the impinging surface. Morris *et al.* (1996) investigated the variation of heat transfer coefficient due to the jet impingement onto the surfaces. They showed that the failure in prediction of near wall effect in turbulence modeling resulted in 16-20 per cent deviation of the mean velocity from the experiment. Turbulence model assessment for jet impingement onto a flat surface was carried out by Cooper *et al.* (1993). They indicated that the standard *k-e* model predicted excessive kinetic energy generation near the wall. Fully developed jets impinging onto a constant heat flux surface was examined by Elison and Webb (1994). They showed that for fully developed jet impinging situation, the Nusselt number was not greatly influenced by the nozzle-to-plate spacing. A turbulent jet impingement onto a surface and a local heat transfer were investigated by Wolf *et al.* (1995). They noted that the velocity gradient along the impinging surface was jet Reynolds number dependent and it changed linearly with increasing nozzle-to-plate spacing. The jet impingement onto a flat plate and heat transfer were studied by Huang and El-Genk (1994). They showed that the jet spacing had significant effect on the flow structure above the flat surface influencing the heat transfer rates considerably. Yilbas *et al.* (2004) investigated jet impingement onto a cavity. They demonstrated that the heat transfer coefficent increased in the exit region of the cavity wall because of radial acceleration of the flow. Sunden *et al.* (2004) studied jet impingement and forced convection cooling of gas turbine components. They showed that the crossflow was squized under the jet; in which case, heat transfer coefficient was reduced. Immarigeon and Hassan (2006) investigated impingement/film cooling of gas turbine components. They showed that the new cooling scheme combined the advantages of traditional film cooling with that of impingement cooling. The heat treatment process through quenching of individual metallic parts with multiple gas jets was examined by Heck *et al.* (2001). They indicated that the optimum hardenining of the surface was possible with proper setting of the nozzle location and operating conditions. Shuja *et al.* (2002, 2005a, b) studied jet impingement onto the heated surfaces and the cavities. They showed that the geometric configurations of the nozzle highly influenced the heat transfer rates from the impinging surfaces and cavities.

However, in the early studies (Shuja *et al.*, 2002, 2005a,b), the effect of nozzle exit velocity together with the conical nozzle cone angle on the flow structure and heat transfer rates was left obscure. Consequently, investigation into effects of nozzle exit velocity together with the cone angle of the conical nozzle on the flow field becomes essential.

In the present study, flow emerging from a conical nozzle and impinging onto a cylindrical cavity resembling the laser machining situation is considered and the effect of nozzle exit velocity and the cone angle of the nozzle on the flow structure and transfer rates within the cylindrical cavity is examined. A numerical scheme accommodating the control volume approach is introduced to solve the governing equations of flow and heat transfer numerically. The Reynolds stress model (RSM) is employed in the analysis to account for the turbulence.

2. Mathematical modelling

The jet emerging from a conical nozzle satisfies the steady flow conditions. The compressibility and variable properties of the working are accommodated when simulating the jet impingement onto the cylindrical cavity. The heat source with a constant heat flux is considered at the cavity surface. The schematic view of the nozzle and the conical cavity is shown in Figure 1, while geometric arrangements of the conical nozzle and the cavity are shown in Figure 2, whereas the nozzle and the cavity configurations are given in Tables I and II, respectively.

2.1 Flow equations

The governing flow and energy equations for the axisymmetric impinging jet can be written in the Cartesian tensor notation as

(i) the continuity equation

$$\frac{\partial}{\partial x_i}(\rho U_i) = 0; \tag{1}$$

(ii) the momentum equation

$$\frac{\partial}{\partial x_i}(\rho U_i U_j) = -\frac{\partial p}{\partial x_j} + \frac{\partial}{\partial x_i}\left[\mu\left(\frac{\partial U_i}{\partial x_j} + \frac{\partial U_j}{\partial x_i}\right) - \rho R_{ij}\right] \tag{2}$$

(iii) and the energy equation

$$\frac{\partial}{\partial x_i}(\rho U_i H) = \frac{\partial}{\partial x_i}\left[\frac{\mu}{\sigma}\frac{\partial H}{\partial x_i} - \rho R_{ih}\right] \tag{3}$$

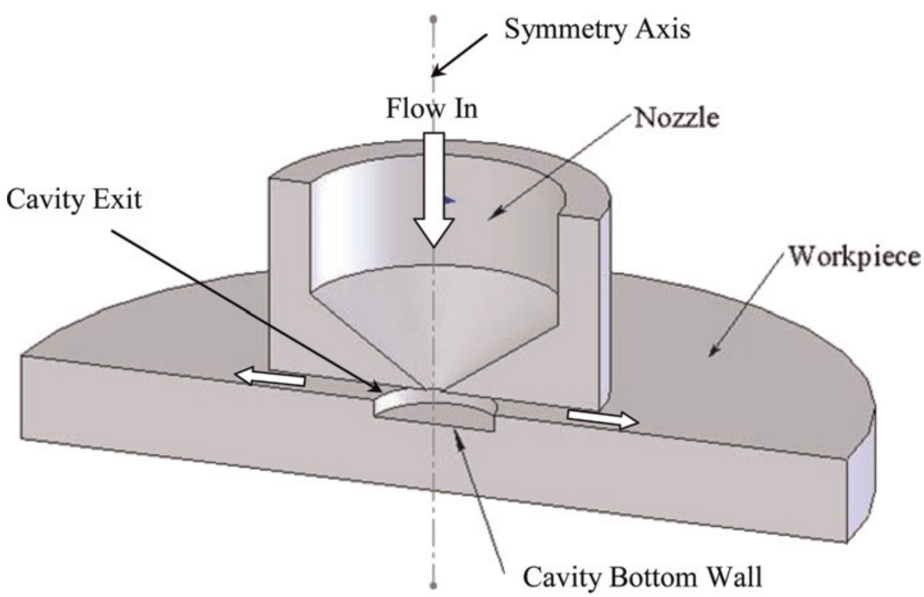

Figure 1. Three-dimensional view of conical nozzle and cylindrical cavity

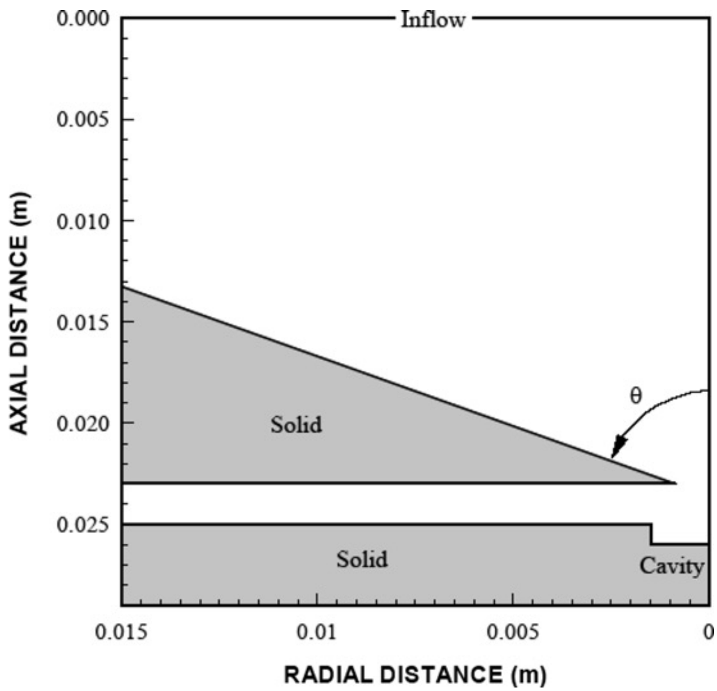

Figure 2.
Solution domain of nozzle and the cavity

Table I.
Geometric configuration of conical nozzle

Nozzle no.	Cone angle, θ(deg)
1	55
2	70

Table II.
Size and depth of the cavity

Cavity diameter (m)	Cavity depth (m)
0.003	0.0005
0.003	0.001

When modelling the Reynolds stresses and turbulence properties the following steps are considered. The RSM is based on the second-moment closure. The transport equation of the Reynolds stress (R_{ij}) is

$$\frac{\partial}{\partial x_m}(U_m R_{ij}) = P_{ij} + \Lambda_{ij} - \epsilon_{ij} + \Pi_{ij} + \Pi_{ij}^w \qquad (4)$$

where P, Λ, ϵ, Π and Π^w are the rate of production, transport by diffusion, rate of dissipation, transport due to turbulent pressure excluding strain interactions and transport due to wall reflection, respectively. Equation (4) consists of six partial differential equations; one for the transport of each of the six independent Reynolds stresses. The production term (P_{ij}), diffusion (Λ_{ij}), dissipation (ϵ_{ij}), transport due to turbulent pressure (Π_{ij}) and the modelling of the wall reflection (Π_{ij}^{w}) are referred to Launder (1989).

2.2 Flow boundary conditions

Four boundary conditions are considered in accordance with the geometric arrangement of the problem, as shown in Figure 2.

2.2.1 Solid wall. For the solid wall, the no-slip condition is assumed at the solid wall, and the boundary condition for the velocity at the solid wall therefore is

$$U_i = 0. \tag{5}$$

2.2.2 Generalized wall functions for normal and shear turbulent stresses for the RSTM model. When the flow is very near the wall, it undergoes a rapid change in direction, the wall-functions approach is not successful in reproducing the details of the flow. Consequently, the turbulent stresses and fluxes at the near-wall grid points are calculated directly from their transport equations. In this case, the near-wall region lying between the wall and the near-wall computational node at x_p can be represented by two layers: the fully viscous sublayer, defined by $\mathrm{Re}_v = x_v\sqrt{k_v}/\nu \simeq 20$, and a fully-turbulent layer. The wall shear stress near the wall is employed, i.e. $\overline{vw}|_{z_v} = \tau_w/\rho$, which serves as the boundary condition for the $\overline{vw}$transport equation.

In relation to normal stresses, the turbulence energy must decrease quadratically towards a value of zero at the wall, therefore, a zero-gradient condition for the normal stresses is physically realistic. This situation is insufficient to ensure an accurate numerical representation of near-wall effects. An improved approach for internal cells is needed in respect of evaluating volume-integrated production and dissipation of normal stresses (these are normally evaluated at cell centres, using linear interpolation and then multiplied by the cell volume). Considering $\overline{v^2}$as an example, the volume-integrated production of $\overline{v^2}$ between the wall and the P-node may be approximated by,

$$\int_{\Delta r}\int_{0}^{z_p} P_{22}\,d\forall \cong \int_{\Delta r}\int_{x_v}^{x_p} -2\overline{vw}\frac{\partial V}{\partial x}\,d\forall = 2\tau_w\left(\frac{V_p - V_v}{x_p - x_v}\right)x_p\Delta r; \tag{6}$$

where V_p and V_v follow from the log-law. No contribution arises from the viscous sublayer, since $\overline{vw} = 0$ in this layer. An analogous integration of the dissipation rate with the assumptions,

$$\epsilon = \frac{2\nu k_v}{x_v^2} \qquad 0 \le x \le x_v,$$
$$\epsilon = \frac{C_\mu^{3/4}k_p^{3/2}}{\kappa x_v} \qquad x_v \le x < x_p,$$

leads to

$$\int_{\Delta r}\int_{0}^{x_p} \epsilon\,d\forall \cong \left[\frac{2\nu k_p}{x_v} + \frac{C_\mu^{3/4}k_p^{3/2}}{\kappa}ln\left(\frac{x_p}{x_v}\right)\right]\Delta r, \tag{7}$$

an analogous treatment is applied to $\overline{v^2}$, while the production of $\overline{w^2}$ in the viscous and turbulent near wall layers region is zero.

The values resulting from equations (6) and (7) are added, respectively, to the volume-integrated generation and dissipation computed for the upper half of the near-wall volume.

It should be noted that for the wall-law approach, the near-wall dissipation (ϵ_p) is not determined from its differential equation applied to the near-wall cell surrounding the node. Instead, and in accordance with the log law, this value is obtained via the length scale from $\epsilon_p = C_\mu^{3/4} k_p^{3/2} / \kappa z_p$, which serves as the boundary conditions for inner cells.

2.2.3 Inlet conditions. The boundary conditions for temperature and the mean jet velocity at the nozzle exit is introduced. Therefore, at the nozzle exit: T = specified (300 K) and the values of the mean jet velocity at the nozzle exit are shown below (mean jet velocity, V_j (m/s)):

- 25
- 50
- 75
- 100

The values of k and ϵ are not known at the inlet, but can be determined from the turbulent kinetic energy i.e.

$$k = \lambda \overline{u}^2, \tag{8}$$

where $\overline{u}$ is the average inlet velocity and λ is a percentage.

The dissipation is calculated from $\epsilon = C_\mu k^{3/2} / aD$, where D is the diameter. The values $\lambda = 0.03$ and $a = 0.005$ are commonly used and may vary slightly in the literature Elkaim *et al.* (1992).

2.2.4 Outlet. The flow is considered to be extended over a long domain; therefore, the boundary condition (outflow boundaries, Figure 2) for any variable ϕ is

$$\frac{\partial \phi}{\partial x_i} = 0, \tag{9}$$

where x_i is the normal direction at outlet.

2.2.5 Symmetry axis. At the symmetry axis, the radial derivative of the variables is set to zero, i.e.

$$\frac{\partial \phi}{\partial r} = 0, \tag{10}$$

except for

$$V = \overline{vw} = \overline{vh} = \overline{wh} = 0. \tag{11}$$

2.3 Solid side

2.3.1 Constant wall temperature boundary. Two constant temperature boundaries are considered. The first one is in the radial direction far away from the symmetry axis at a constant temperature $T = T_{amb}(300\,\text{K})$. It should be noted that the constant temperature boundary condition is set at different locations in the radial directions. The boundary condition (T = constant) located in the radial direction had no significant effect on the temperature and flow field in the stagnation region. Therefore, this boundary condition is set for a radial distance of 0.015 m from the symmetry axis. The second constant temperature boundary is set at the cavity walls (as shown in Figure 2) at T = constant (1,500 K).

2.3.2 Solid fluid interface. The coupling of conduction within the solid and convection within the fluid, termed conjugation, is required for the present analysis at the solid fluid interface. The appropriate boundary conditions are continuity of heat flux and temperature and are termed boundary conditions of the fourth kind. i.e.

$$T_{w_{\text{solid}}} = T_{w_{\text{gas}}} \textit{ and } K_{w_{\text{solid}}} \frac{\partial T_{w_{\text{solid}}}}{\partial x} = K_{w_{\text{gas}}} \frac{\partial T_{w_{\text{gas}}}}{\partial x}. \tag{12}$$

No radiation losses from the solid surface is assumed.

2.4 Gas properties

The equation of state is used for air and the properties employed are given in Table III.

3. Numerical method and simulation

A control volume approach is employed when discretizing the governing equations. The discretization procedure is given in Patankar (1980). The problem of determining the pressure and satisfying continuity may be overcome by adjusting the pressure field so as to satisfy continuity. A staggered grid arrangement is used in which the velocities are stored at a location midway between the grid points, i.e. on the control volume faces. All other variables including pressure are calculated at the grid points. This arrangement gives a convenient way of handling the pressure linkages through the continuity equation and is known as semi-implicit method for pressure-linked equations algorithm. The details of this algorithm are given in Patankar (2000).

The computer program used for the present simulation can handle a non-uniform grid spacing. In each direction fine grid spacing near the gas jet impinging point and the cavity is allocated while gradually increased spacing for locations away from the cavity is considered. Elsewhere, the grid spacing is adjusted to maintain a constant ratio of any of two adjacent spacings. The grid generated in the present study is shown in Figure 3. The number of grid planes used normal to the x and r directions are 220 and 272, respectively, for the pipe and the conical nozzle. The grid independence tests were conducted and it is observed that the grid selected results in the grid-independent solution.

Nine variables are computed at all grid points; these are: two velocity components, local pressure, five turbulence quantities and the temperature.

Density	ρ (kg m^{-3})	p/RT
Thermal conductivity	K (W m^{-1} K^{-1})	0.0242
Specific heat capacity	c_p (J kg^{-1} K^{-1})	1,006.43
Viscosity	ν (kg m^{-1} s^{-1})	1.7894×10^{-5}

Table III. Air properties used in the simulation

4. Results and discussions

Jet emerging from a conical nozzle and impinging onto a cylindrical cavity resembling the laser machining situation is considered. The influence of jet velocity and nozzle cone angle on the resulting flow field and heat transfer rates is examined. The cavity wall was kept at almost the melting temperature of the substrate material as similar to the laser produced cavity temperature. Two cavity depths are considered and air is employed as the working fluid in the simulations.

Figure 4 shows comparison of the predictions and the experimental data obtained from the previous study (Cooper *et al.*, 1993) for normalized velocity magnitude along the axial distance at normalized radial location is $r/D = 0.5$, where D is the nozzle diameter. Velocity magnitude is normalized with the mean jet velocity at the nozzle exit. The experimental data were obtained for the jet impinging onto the flat plat at the jet $Re = 23{,}000$. The simulation conditions are arranged to resemble the experimental conditions. It can be observed that both results are in good agreement. Therefore, the model adopted in the present study has a sound base to represent the actual flow conditions.

Figure 5 shows contours of normalized velocity magnitude (V/V_j) for different jet exit velocities and two cone angles of the conical nozzle while the cavity depth is 0.5 mm. The effect of nozzle exit velocity on the flow field in the region close to the nozzle is evident, particularly for the cone angle of 55°. In this case, flow emerging from the nozzle expands in the radial direction before impinging onto the surface. The flow generated from the cavity due to the impinging jet expands radially and forms the streamline curvatures. The radially expanded jet and the flow emanated from the cavity results in high shear rates within the vicinity of the jet outer surface. This, in turn, results in the formation of a circulation cell in this region. As the nozzle exit velocity increases, the shear rate increases and the size as well as the orientation of the circulation cell changes. This is more pronounced for the nozzle cone angle of 55°.

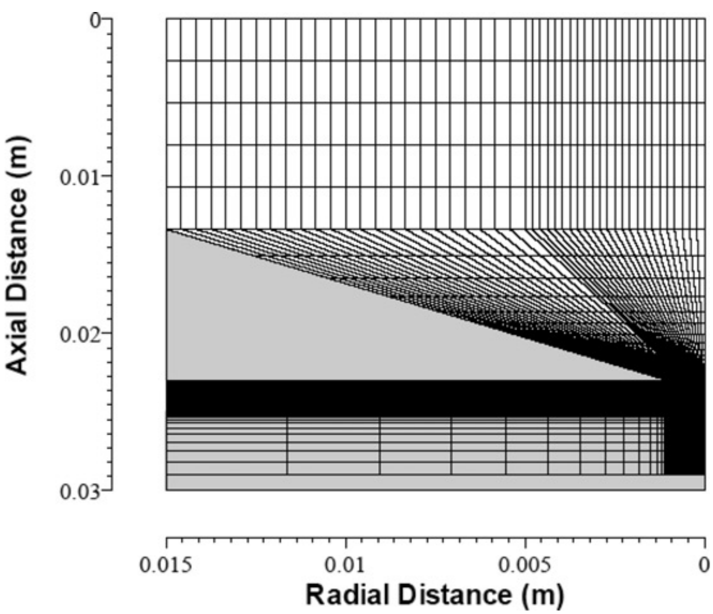

Figure 3.
Grid used in the simulations

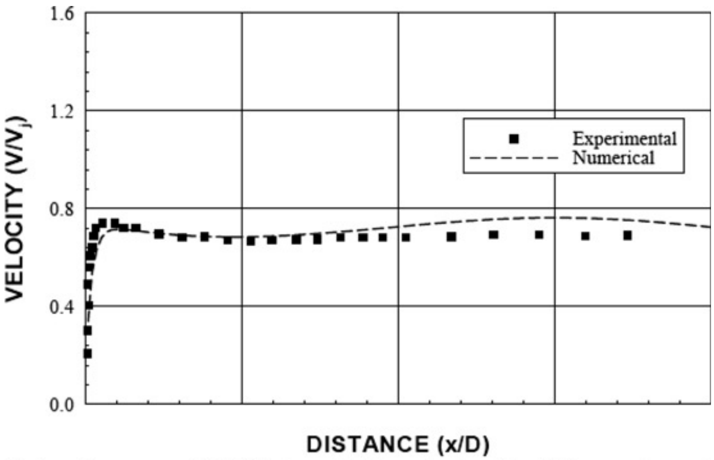

Notes: Cooper *et al.*(1993); the radial location is $r/D = 0.5$; experimental conditions are used in the simulations – in which case, flow impinging onto a flat plate is simulated for Re = 23000

Figure 4. Normalized velocity distribution along the dimensionless distance corresponding to predictions and the experiment

However, flow mixing due to radial expansion of the jet, onset of leaving the nozzle, and the flow emanated from the cavity, because of the impinging jet, develops a complicated flow structure around the edges of the cavity. This situation is also seen in the previous study (Yilbas *et al.*, 2004). In the case of the deep cavity (1 mm depth) (Figure 5*b*), similar situation is observed, provided that the radial expansion of the flow emanating from the cavity, due to jet impingement, is small and the shear strain between the impinging jet and the flow emanating from the cavity does not generate a circulation cell in the region of the jet outer boundary. Moreover, the impinging jet in the cavity causes the stream line curvature, due to radial expansion in the cavity. This increases the rate of fluid strain in the cavity, particularly in the region close to the cavity bottom. This is more pronounced for high jet velocities and large cone angles. Consequently, small circulation cell is formed in this region.

Figure 6 shows normalized temperature (T/T_j) contours for different jet velocities at nozzle exit and two nozzle cone angles while the cavity depth is 0.5 mm. Temperature contours follow almost the velocity profiles provided that, in the region close to the cavity walls, temperature attains high values due to the consideration of elevated wall temperature resembling the laser machining conditions. Since air (working fluid) is considered as an ideal gas, the thermodynamic pressure developed in the thermal boundary layer in the cavity wall region contributes significantly to the flow structure in the region next to the thermal boundary. This influences the radial flow and enhances the rate of fluid strain in the region next to the thermal boundary layer. This situation is more pronounced for the low-velocity jet at nozzle exit. Consequently, the flow emanating from the cavity in the region close to the cavity exit attains high-temperatures. Moreover, increasing the nozzle cone angle influences this situation in such a way that the radial accelerated flow in the streamline curvature mixes with the high-temperature fluid above the cavity inlet causing further extension of the high-temperature region. Increasing jet velocity suppresses the thermal boundary layer thickness in the cavity. However, increasing the cavity depth (Figure 6(*b*)) enhances the thermal boundary layer in the cavity. This, in turn, enhances the extension of the high-temperature region above the cavity towards the cavity edge. The

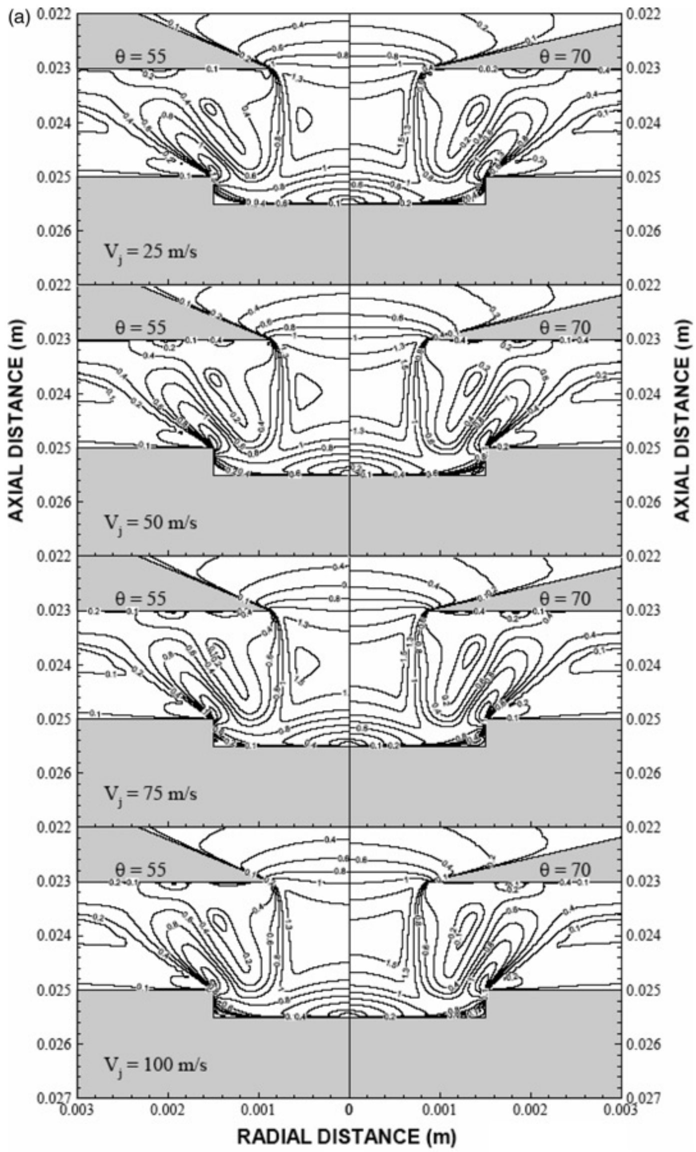

(a) Normalized velocity magnitude contours for different jet velocities at the nozzle exit and two nozzle angles at cavity depth of 0.5 mm

Figure 5.
Normalized velocity magnitude contours

(*continued*)

streamline curvature developed for the shallow cavity (Figure 6(*a*)) suppress the radial expansion of the flow emanating from the cavity and modifies the flow mixing above the cavity surface. This in turn, alters the temperature field above the cavity away from the symmetry axis.

Figure 7 shows the Nusselt number variation along the cavity bottom wall for two cavity depths and nozzle cone angles while nozzle exit velocity is variable. The location of radial distance 0.0 represents the symmetry axis at the cavity wall. The Nusselt

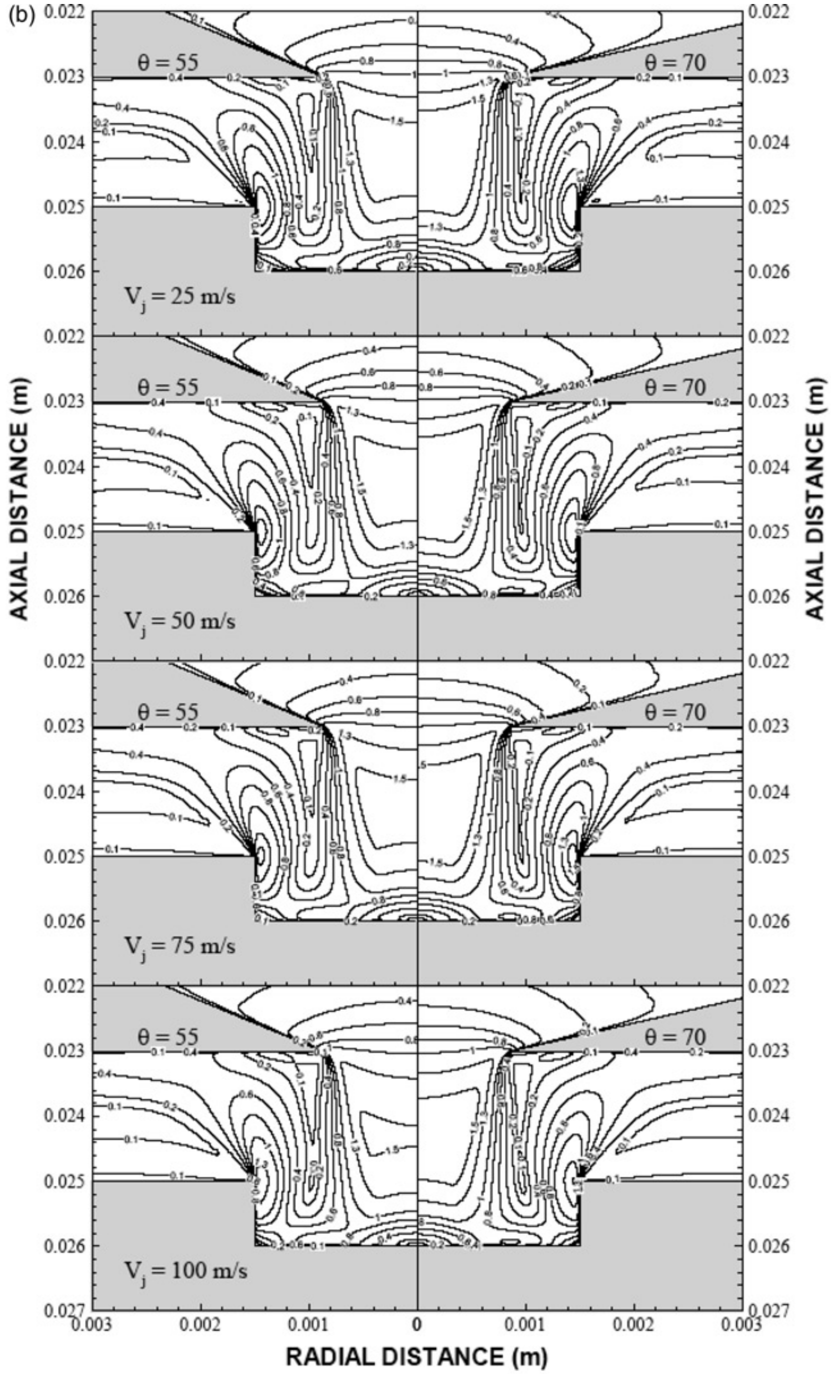

Figure 5.

(b) Normalized velocity magnitude contours for different jet velocities at the nozzle exit and two nozzle angles at cavity depth of 1 mm

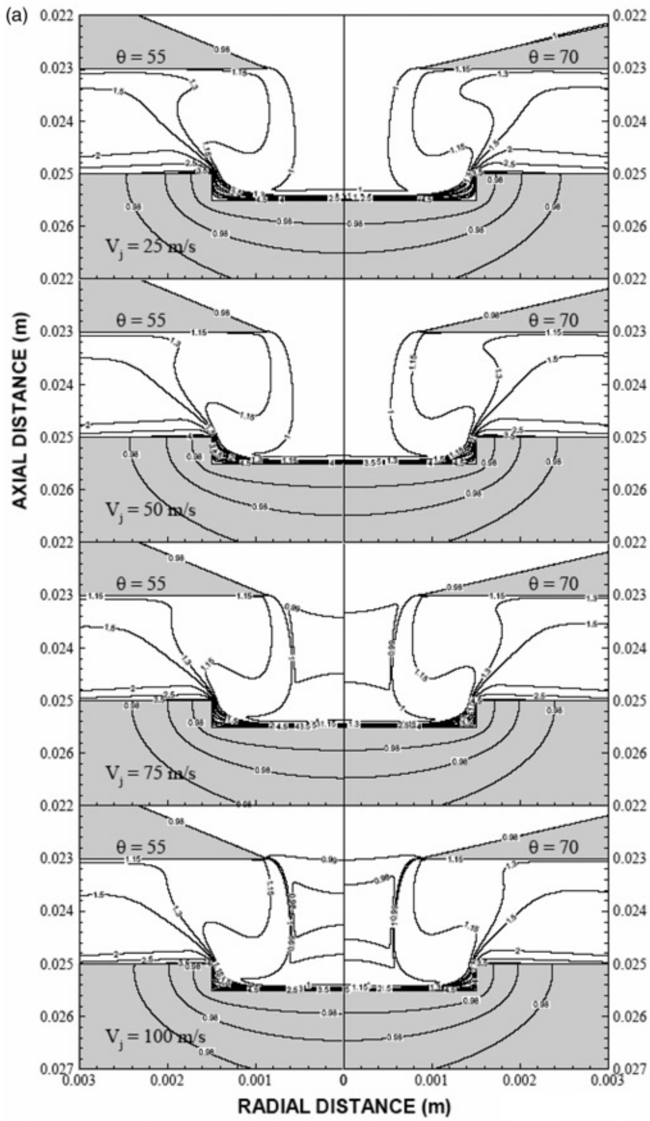

Figure 6.
Normalized temperature contours

(a) Normalized temperature contours for different jet velocities at the nozzle exit and two nozzle angles at cavity depth of 0.5 mm

(*continued*)

number attains high values in the region of symmetry axis and as the radial distance increases towards the cavity wall, it reduces gradually. The attainment of the high Nusselt number is associated with the flow structure developed in the cavity. The pressure region developed in the cavity along the cavity symmetry axis, due to jet impingement into cavity, results in a radial flow towards the cavity wall. This in turn, enhances the convective cooling of the surface in the region around the symmetry axis. Moreover, in the edges of the cavity wall, thermodynamic pressure developed because

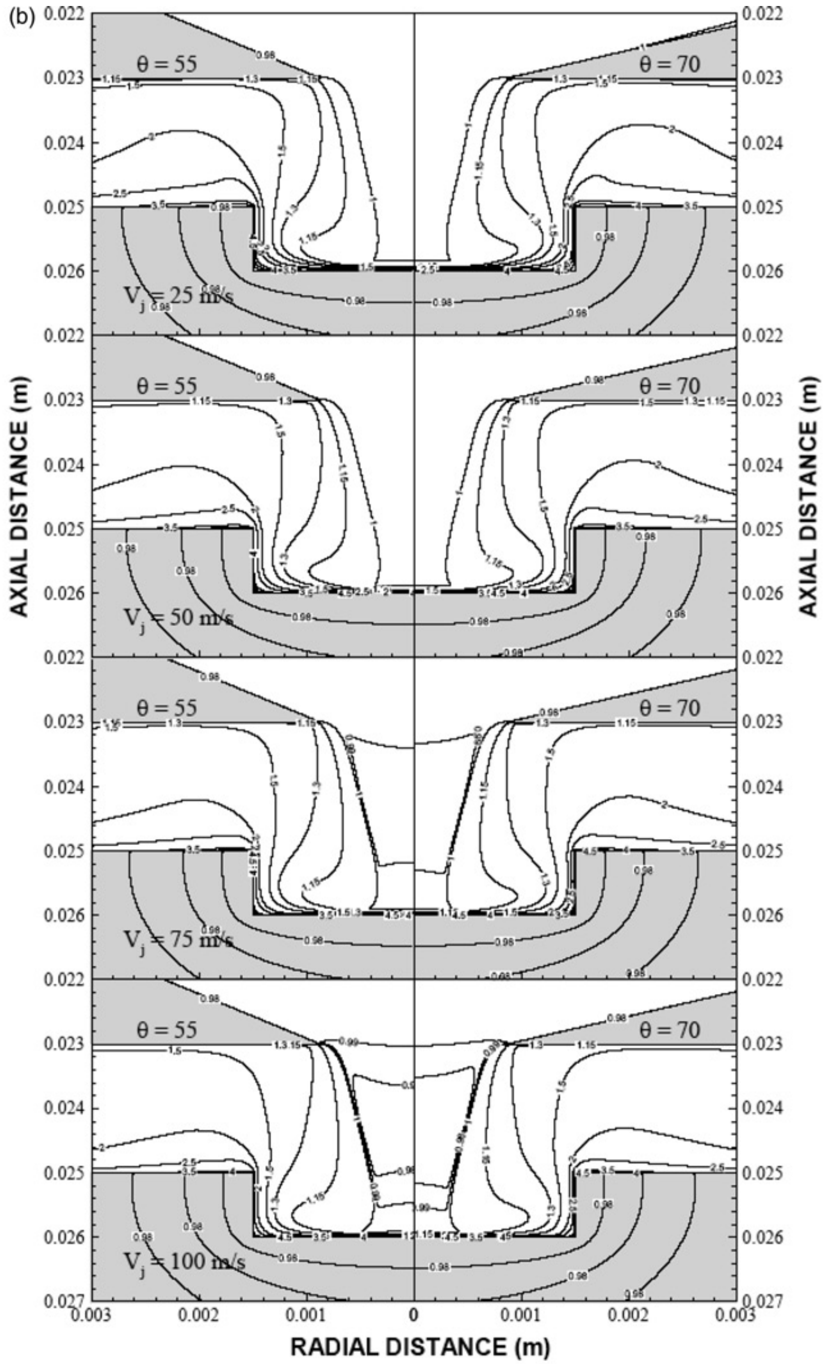

Figure 6.

(b) Normalized temperature contours for different jet velocities at the nozzle exit and two nozzle angles at cavity depth of 1 mm

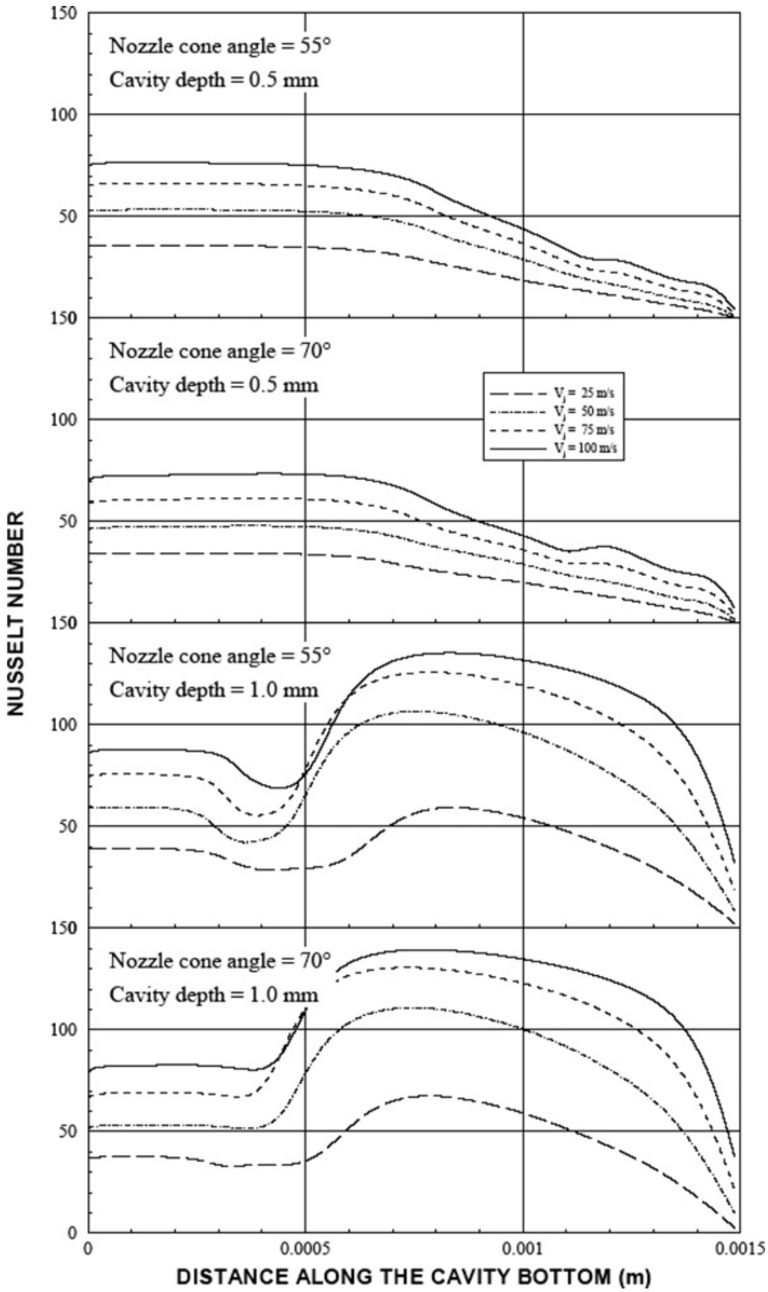

Figure 7.
Nusselt number along the cavity bottom for different jet velocities at the nozzle exit and two nozzle angles as well as cavity depths

of high wall temperature lowers the flow velocity in this region. However, due to streamline curvature, flow mixing is suppressed in this region. This is particularly true for the shallow cavity (cavity depth is 0.5 mm) for the both nozzle cone angles. Moreover, the influence of nozzle cone angle on the Nusselt number is not significant.

The influence of nozzle exit jet velocity on the Nusselt number is significant, in which case, increasing jet velocity improves significantly the Nusselt number, particularly in the region of the symmetry axis. In the case of the cavity with depth of 1 mm, the Nusselt number behavior changes form that of 0.5 mm depth. The Nusselt number attains low values in the neighborhood of the symmetry axis and as the radial distance increases from the symmetry axis, it attains high values, provided that the sharp decay occurs in the vicinity of the cavity wall ($r > 1.25 \times 10^{-3}$ m). Increase in the Nusselt number at the cavity bottom wall is because of the complex flow structure developed in this region. As the cavity depth increases, the stagnation zone moves into the cavity, this in turn modifies the streamline curvature of the impinging jet in the cavity. Consequently, the radial flow developed within the region close to the bottom of the cavity is responsible for the enhancement of the Nusselt number. Due to the influence of the stagnation zone within the region of the symmetry axis, the Nusselt number attains lower values as compared to the region in its near neighborhood.

Figure 8 shows the skin friction coefficient in the region close to the bottom of the cavity. The skin friction remains low in the region of the symmetry axis and it increases in the radial direction in the region next to the symmetry axis. This is because of the rate of fluid, which increases with the radial distance in this region. Moreover, close to the cavity wall ($1.25 \times 10^{-3}\,\text{m} < r < 1.5 \times 10^{-3}$ m), the skin friction reduces significantly due to the creeping like flow developed in this region. As the depth of the cavity increases (cavity depth is 1 mm), the radial flow is generated in the cavity because of the stagnation zone formed along the symmetry axis and the streamline curvature effect of the impinging jet. Consequently, the radial flow results in the high rate of the fluid strain in the vicinity of the bottom of the cavity enhancing the skin friction in this region. The influence of the nozzle cone angle on the skin friction is more pronounced for the deeper cavity than that of the shallow cavity. In this case, increasing cone angle enhances the value of the skin friction. This is because of the stagnation zone, which moves slightly towards the entrance of the cavity for the large apex angle of the nozzle. It should be noted that the stagnation zone moves into the cavity for small cone angles (small apex angle of the nozzle). Increasing jet velocity enhances the skin friction, particularly for the large cone angle and deep cavity. In this case, the convective current in the vicinity of the cavity bottom increases with increasing jet velocity. This in turn, enhances the rate of fluid strain in this region, as a consequence, the skin friction increases.

5. Conclusions

Jet impinging onto a cylindrical cavity is considered and the effects of jet velocity at the nozzle exit and nozzle cone angle on the flow field and heat transfer rates from the cavity wall are investigated. Temperature of the cavity wall was kept at almost the melting temperature of the substrate material to resemble the laser produced cavity. In the simulations, two cone angles of conical nozzle, two cylindrical cavity depths, and four jet velocities at the nozzle exit are considered while air is employed as the working fluid. The effect of nozzle exit velocity on the flow structure is significant, particularly in the cavity entrance region. In this case, increasing nozzle exit velocity results in the stagnation region moving further into the cavity. This, in turn, modifies the stream line curvature in the region next to the symmetry axis. This situation is more pronounced for the deep cavity (the cavity depth is 1 mm). The radial flow developed in the deep cavity enhances the heat transfer rates from the bottom surface of the cavity; in which

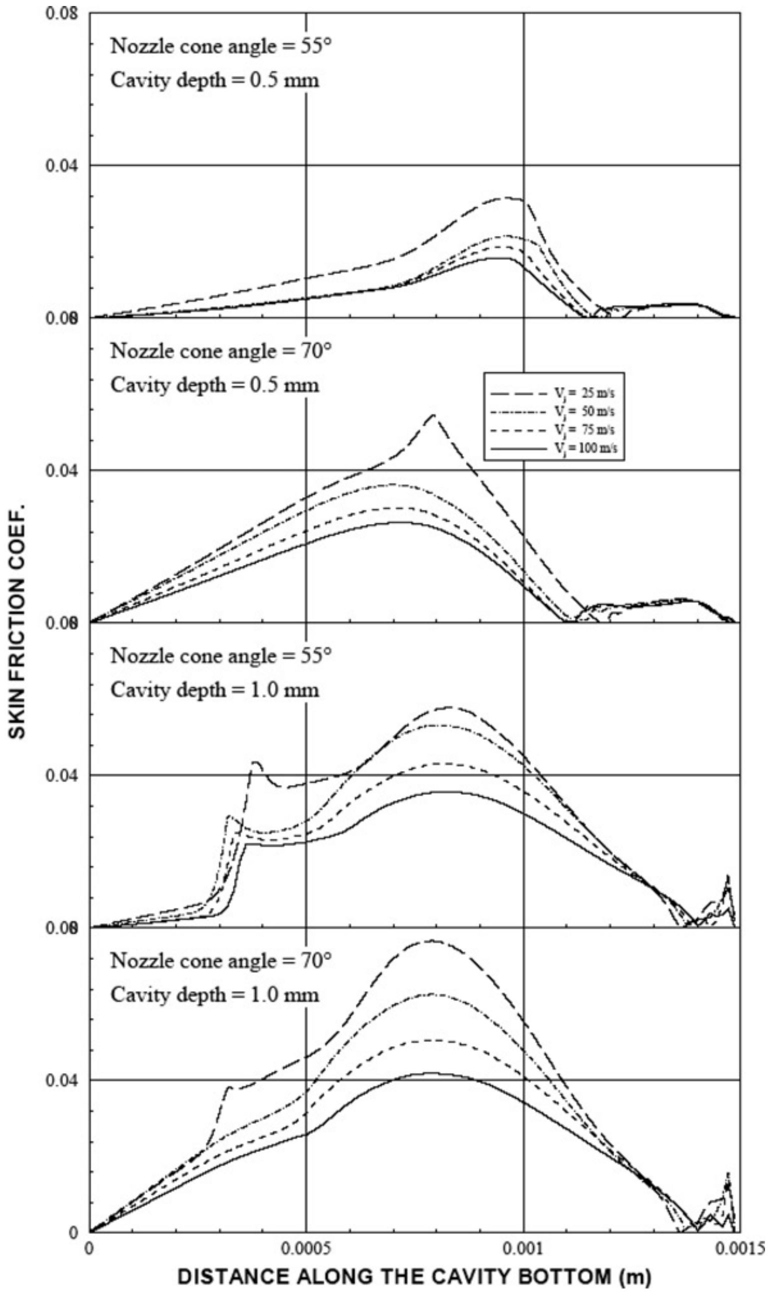

Figure 8.
Skin friction along the cavity bottom for different jet velocities at the nozzle exit and two nozzle angles as well as cavity depths

case, the Nusselt number increases, in particular in the region next to the symmetry axis. The effect of nozzle cone angle on the Nusselt number is not significant for all cavity depths considered in the present study. However, the nozzle cone angle modifies the skin friction at the bottom surface of the cavity such that the skin friction increases for the large nozzle cone angle. The skin friction attains low values in the region of the symmetry axis because of the stagnation zone developed by the impinging jet. However, the radial flow and the streamline curvature enhance the rate of fluid strain in the region of the cavity bottom. This, in turn, increases the skin friction in the region between the symmetry axis and the cavity wall.

References

Ashforth-Frost, S. and Jambunathan, K. (1996), "Numerical prediction of semi-confined jet impingementand comparisons with experimental data", *International Journal of Numerical Methods in Fluids*, Vol. 23, pp. 295-306.

Chen, S.L. (1998), "The effects of gas composition on the co2 laser cutting of mild steel", *Journal of Material Processing Technology*, Vol. 73, pp. 147-59.

Cooper, D., Jackson, D.C., Launder, B.E. and Liao, G.X. (1993), "Impinging jet studies for turbulence model assessment-I: flow-field experiments", *International Journal of Heat and Mass Transfer*, Vol. 36 No. 36, pp. 2675-84.

Elison, B. and Webb, B.W. (1994), "Local heat transfer to impinging liquid jets in the initially laminar, transitional, and turbulent regimes", *International Journal of Heat and Mass Transfer*, Vol. 37 No. 8, pp. 1207-16.

Elkaim, D., Reggio, M. and Camarero, R. (1992), "Simulating two-dimensional turbulent flow by using the k-ε model and the vorticity-stream function formulation", *International Journal for Numerical methods in Fluids*, Vol. 14, pp. 961-80.

Heck, U., Fritsching, U. and Bauckhage, K. (2001), "Fluid flow and heat transfer in gas jet quenching of a cylinder", *International Journal of Numerical Methods for Heat and Fluid Flow*, Vol. 11, pp. 36-49.

Huang, L. and El-Genk, M.S. (1994), "Heat transfer of an impinging jet on a flat surface", *International Journal of Heat and Mass Transfer*, Vol. 37 No. 13, pp. 1915-23.

Immarigeon, A. and Hassan, I. (2006), "Fluid flow and heat transfer in gas jet quenching of a cylinder", *International Journal of Numerical Methods for Heat and Fluid Flow*, Vol. 16, pp. 470-93.

Launder, B.E. (1989), "Second-moment closure and its use in modelling turbulent industrial flows", *International Journal for Numerical Methods in Fluids*, Vol. 9, pp. 963-85.

Man, H.C., Duan, J. and Yue, T.M. (1997), "Design and characteristic analysis of supersonic nozzles for high gas pressure laser cutting", *Journal of Materials Processing Technology*, Vol. 63, pp. 217-22.

Morris, G.K. Gaimella, S.V. and Amano, R.S. (1996), "Prediction of jet impingement heat transfer using a hybrid wall treatment with different turbulent prandtl number functions", *Journal of Heat Transfer*, Vol. 118, pp. 562-9.

Patankar, S.V. (1980), *Numerical Heat Transfer*, McGraw-Hill, New York, NY.

Shuja, S.Z., Yilbas, B.S. and Budair, M.O. (2002), "Laser pulse heating of steel surfaces including impinging gas effect and variable properties", *International Journal of Numerical Methods for Heat and Fluid Flow*, Vol. 12, pp. 195-219.

Shuja, S.Z., Yilbas, B.S. and Budair, M.O. (2005a), "Flow impingement onto a flat plate with limited heated area in relation to laser gas assisted processing: influence of nozzle geometry on heat transfer rates", *International Journal of Numerical Methods for Heat and Fluid Flow*, Vol. 15, pp. 363-78.

Shuja, S.Z., Yilbas, B.S. and Budair, M.O. (2005b), "Influence of conical and annular nozzle geometric configurations on flow and heat transfer characteristics due to flow impingement onto a flat plate", *Numerical Heat Transfer, Part A*, Vol. 48, pp. 917-39.

Sunden, B., Jia, R. and Abdon, A. (2004), "Computation of combined turbulent convective and impringement heat transfer", *International Journal of Numerical Methods for Heat and Fluid Flow*, Vol. 14 No. 1, pp. 116-33.

Wolf, D.H., Viskanta, R. and Incropera, F.P. (1995), "Turbulence dissipation in a free-surface jet of water and its effects on local impingement heat transfer from a heated surface: part 2- local heat transfer", *ASME Journal of Heat Transfer*, Vol. 117, pp. 95-103.

Yilbas, B.S. and Aleem, B.J.A. (2006), "Dross formation during laser cutting process", *Journal of Physics Part D: Applied Physics*, Vol. 39, pp. 1451-61.

Yilbas, B.S., Shuja, S.Z. and Budair, M.O. (2002), "Jet impingement onto a cavity", *International Journal of Numerical Methods for Heat and Fluid Flow*, Vol. 12, pp. 817-38.

Yilbas, B.S., Shuja, S.Z. and Budair, M.O. (2004), "Jet impingement onto a conical cavity with elevated wall temperature", *International Journal of Numerical Methods for Heat and Fluid Flow*, Vol. 14, pp. 1011-28.

Corresponding author
B.S. Yilbas can be contacted at: bsyilbas@kfupm.edu.sa